Structure guided design of a series of selective pyrrolopyrimidinone MARK Inhibitors

Jason D. Katz, Andrew Haidle, Kaleen K. Childers, Anna A. Zabierek, James P. Jewell, Yongquan Hou, Michael D. Altman, Alexander Szewczak, Dapeng Chen, Andreas Harsch, Mansuo Hayashi, Lee Warren, Michael Hutton, Hugh Nuthall, Hua-Poo Su, Sanjeev Munshi, Matt G. Stanton, Ian W. Davies, Ben Munoz, Alan Northrup

PII: S0960-894X(16)30900-3
DOI: http://dx.doi.org/10.1016/j.bmcl.2016.08.068
Reference: BMCL 24194

To appear in: *Bioorganic & Medicinal Chemistry Letters*

Received Date: 13 July 2016
Revised Date: 19 August 2016
Accepted Date: 20 August 2016

Please cite this article as: Katz, J.D., Haidle, A., Childers, K.K., Zabierek, A.A., Jewell, J.P., Hou, Y., Altman, M.D., Szewczak, A., Chen, D., Harsch, A., Hayashi, M., Warren, L., Hutton, M., Nuthall, H., Su, H-P., Munshi, S., Stanton, M.G., Davies, I.W., Munoz, B., Northrup, A., Structure guided design of a series of selective pyrrolopyrimidinone MARK Inhibitors, *Bioorganic & Medicinal Chemistry Letters* (2016), doi: http://dx.doi.org/10.1016/j.bmcl.2016.08.068

Graphical Abstract

To create your abstract, type over the instructions in the template box below.
Fonts or abstract dimensions should not be changed or altered.

Structure Guided Design of a Series of Selective Pyrrolopyrimidinone MARK Inhibitors

Leave this area blank for abstract info.

Jason D. Katz, Andrew Haidle, Kaleen K. Childers, Anna A. Zabierek, James P. Jewell, Yongquan Hou, Michael D. Altman, Alexander Szewczak, Dapeng Chen, Andreas Harsch, Mansuo Hayashi, Lee Warren, Michael Hutton, Hugh Nuthall, Hua-Poo Su, Sanjeev Munshi, Matt G. Stanton, Ian W. Davies, Ben Munoz, and Alan Northrup

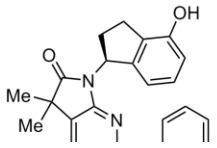

MARK3 IC_{50} = 1.2 nM
MARK4 Cell IC_{50} = 21 nM

ELSEVIER

Bioorganic & Medicinal Chemistry Letters
journal homepage: www.elsevier.com

Structure guided design of a series of selective pyrrolopyrimidinone MARK Inhibitors

Jason D. Katz, [a*] Andrew Haidle,[a] Kaleen K. Childers,[a] Anna A. Zabierek,[a] James P. Jewell,[a] Yongquan Hou,[a] Michael D. Altman,[b] Alexander Szewczak,[c] Dapeng Chen,[d] Andreas Harsch,[d] Mansuo Hayashi,[e] Lee Warren,[e] Michael Hutton,[e] Hugh Nuthall,[e] Hua-Poo Su,[f] Sanjeev Munshi,[f] Matt G. Stanton,[a] Ian W. Davies,[a] Ben Munoz,[a] and Alan Northrup[a]

[a] *Department of Chemistry, Merck & Co., 33 Avenue Louis Pasteur, Boston, MA 02115, USA*
[b] *Department of Structural Chemistry, Merck & Co., 33 Avenue Louis Pasteur, Boston, MA 02115, USA*
[c] *Department of In Vitro Sciences, Merck & Co., 33 Avenue Louis Pasteur, Boston, MA 02115, USA*
[d] *Department of Drug Metabolism, Merck & Co., 33 Avenue Louis Pasteur, Boston, MA 02115, USA*
[e] *Department of Neuroscience, Merck & Co., 33 Avenue Louis Pasteur, Boston, MA 02115, USA*
[f] *Department of Structural Chemistry, Merck & Co., 770 Sumneytown Pike, West Point, PA 19486, USA*

ARTICLE INFO

Article history:
Received
Revised
Accepted
Available online

Keywords:
MARK
kinase
Tau
Alzheimer's Disease
Pyrrolopyrimidinone

ABSTRACT

The initial structure activity relationships around an isoindoline uHTS hit will be described. Information gleaned from ligand co-crystal structures allowed for rapid refinements in both MARK potency and kinase selectivity. These efforts allowed for the identification of a compound with properties suitable for use as an *in vitro* tool compound for validation studies on MARK as a viable target for Alzheimer's disease.

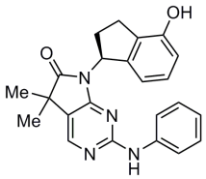

MARK3 IC_{50} = 1.2 nM
MARK4 Cell IC_{50} = 21 nM

Alzheimer's disease (AD) represents a huge unmet medical need that will only become more urgent with the current aging population. In fact, the number of people suffering from this disease has been estimated to reach 13-16 million in the United States alone by 2050(1). However, despite significant efforts from the scientific community, robust disease-modifying therapies for AD have remained elusive(2). A major physiological marker of AD is the abnormal deposit of plaques in the brain, primarily made up of either amyloid Aβ protein or neurofibrillary tangles (NFTs). As such, many of the therapeutic strategies approached to combat AD have focused on reducing the severity of these lesions. Tau binds to and stabilizes microtubules (MTs), particularly in neuronal axons, and thus plays a crucial role in the neuronal cytoskeleton stabilization. Tau can become abnormally hyper-phosphorylated in the AD brain, causing it to lack affinity for MTs and self-associate into NFTs(3). Observations of AD brains show a strong correlation between cognitive dysfunction and cortical NFT density. Moreover, mutations in tau have been shown to cause a form of frontotemporal dementia, which provided a direct genetic link between tau and neurological disease. As such, one therapeutic approach that has been pursued is to decrease the phosphorylation on tau through inhibiting tau kinases, via the hypothesis that this would lead to less tau aggregation.

Multiple kinases are known to phosphorylate tau and many have been examined as possible targets for AD(4). Among them are the microtubule-affinity regulating kinase (MARK) family, consisting of 4 isoforms (MARK1-4). MARKs phosphorylate tau protein in its repeat domain and thereby regulate its affinity for MTs and affect the aggregation of tau into NTFs(5). It was found that PAR-1, the fly homolog of mammalian MARK, directly phosphorylates tau at S262 and S356. This phosphorylation event is a prerequisite for the action of downstream kinases including GSK-3 and Cdk5 to phosphorylate several other sites and generate disease-associated phospho-epitopes(6). Active MARKs are elevated and colocalize with NTFs in the AD brain, and MARK phosphorylation sites on tau are elevated early in transgenic mouse models of tauopathy. These findings suggest that inhibition of MARKs would be an

∗ Corresponding author. Tel.: +1-617-992-2057; fax: +1-617-992-2406; e-mail: jason_katz2@merck.com

attractive therapeutic strategy for the treatment of AD by reducing the levels of unbound tau that are available for the formation of NTFs. In this communication, the initial structure activity relationships around an isoindoline uHTS hit will be described, followed by its evolution into an *in vitro* tool compound. The subsequent communication details the efforts to deliver an *in vivo* tool compound for validation studies on MARK as a viable target for AD.

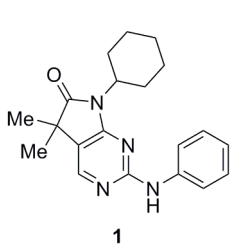

MARK3 IC_{50} = 304 nM
BRSK2 IC_{50} > 10,000 nM
MARK4 cell IC_{50} = 8,600 nM
PGP BA/AB = 0.9
Papp (10^{-6} cm/s) = 12
MW = 336
LE = 0.36
PSA = 55
clogD = 4.06

Figure 1. Properties of uHTS hit compound **1**.

An uHTS screen of the Merck compound collection against MARK3 identified a number of potential starting points for further development. From this set, the team was attracted to a series of pyrrolopyrimidinones, represented by the N-cyclohexyl analog **1** (Figure 1). As a starting point for a CNS program, the initial set of compounds profiled in the class possessed a number of attractive properties, such as a relatively low MW, as well as PSA and clogD values within acceptable ranges(7, 8). In addition, compounds such as **1** proved not to be substrates for Pgp(9). While **1** was not exquisitely potent, by the metrics we were tracking at the time, it was relatively efficient (LE = 0.36) and exhibited a moderate cell shift (28x) (10, 11, 12). Furthermore, there was evidence of baseline selectivity against BRSK2, another kinase capable of phosphorylating Tau(13). Throughout the program, selectivity against a small panels of kinases, including BRSK2 was used to monitor progress against off-targets that could complicate interpretation of downstream target validation experiments. At the time this work was conducted, a key goal for the program was to identify *in vitro* and *in vivo* tool compounds to validate the target. The main focus of this manuscript will be to describe initial efforts in this area.

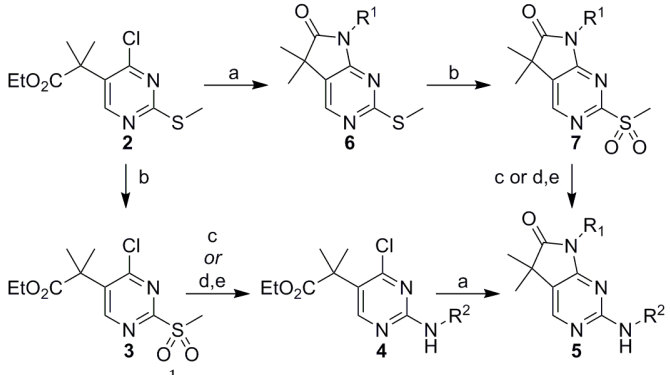

Scheme 1. a) R^1NH_2, DABCO, 2-ethoxyethanol, 140 °C; b) *m*-CPBA, DCM, 20 °C; c) R^2NH_2, NaHMDS, THF, 20 °C; d) R^2NHCHO, NaH, DMF, 0 °C; e) $NaHCO_3$, THF/MeOH/H_2O, 20 °C.

The chemistry to prepare most of the analogs is described in Scheme 1, starting from 2-thiomethylpyrimidine **2**(14). Treatment with m-CPBA provided the sulfone **3**, which was then displaced with an amine to deliver the aminopyrimidine analogs **4**. Subsequent condensation with another primary amine supplied the desired functionalized pyrrolipyrimidinones **5**. Conversely, an alternate sequence of synthetic steps would allow for initial formation of the lactam **6**, followed by oxidation and SNAr to arrive at pyrrolopyrimidinones **5**.

The transposed isoindolinone analog **11** was accessed using the synthetic sequence described in Scheme 2. Commercially available acid **8** could be transformed to the amino pyrimidine **9** using procedures described above (esterification, oxidation to the sulfone, displacement with formanilide, and a Boc protection). The bromide was then converted to the isoprenyl analog followed by transformation of the ester to the pyrazolyl amide **10**. This advanced intermediate was then treated with IBX under the conditions described by Baran and Nicolau (15, 16, 17, 18, 19) followed by Boc deprotection to deliver the highly functionalized isoindolinone **11**. To the best of our knowledge, the IBX methodology in reference 11 has not been previously extended to more complex, dense hetererocyclic systems such as in **11**(20).

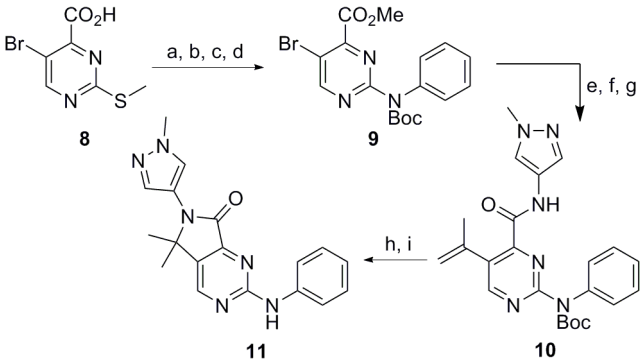

Scheme 2. a) TMS-diazomethane, CH_2Cl_2/MeOH (1:1), *95%;* b) oxone, THF/MeOH/sat'd $NaHCO_3$(aq)/water (1:1:1:1), *86%*; c) formanilide, NaH, DMF, 0 °C→RT, 1 h, *70%*; d) Boc_2O, NEt_3, THF, *quant*; e) isopropenyl boronic acid, pinacol ester, $Pd(OAc)_2$, $^{cy}Hex_3P$, K_3PO_4, toluene/water (3:1), *95%*; NaOH, THF/MeOH (1:1); g) 1-methyl-1*H*-pyrazol-4-amine, BOP-Cl, $^{i}PrNEt_2$, CH_3CN, *60%*; h) IBX, THF/DMSO (10:1), 90 °C, *40%*; i) TFA, CH_2Cl_2, *86%*.

The dihydro-pyrrolopyrimidine **13** was prepared via a slightly modified route (Scheme 3). Treatment of sulfide **6a** (prepared as in Scheme 1, using cyclohexylamine) with lithium aluminum hydride delivered the intermediate aminal, which was further reduced to **12** in the presence of triethysilane. A further 2-step sequence involving oxidation of the sulfide and displacement with aniline allowed for isolation of the fully functionalized **13**.

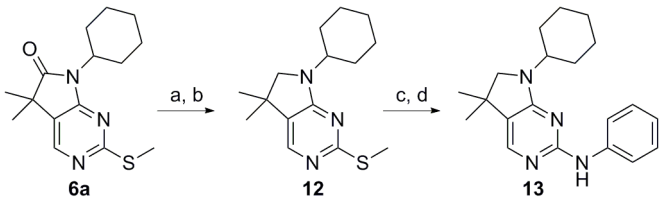

Scheme 3. a) $LiAlH_4$, THF, 0 °C→RT, *92%*; b) $BF_3{\cdot}OEt_2$, Et_3SiH, CH_2Cl_2, -78 °C→RT, *78%*; c) oxone, THF/MeOH/sat'd $NaHCO_3$(aq) (1:1:1); d) aniline, $^{i}PrNEt_2$, 155 °C, *6%* (2 steps).

In addition to the physical properties mentioned above, **1** offered many potential regions for further elaboration. Based on the kinase literature and preliminary modeling studies, it was assumed that these compounds bound to the ATP binding pocket of the kinase, where the amino pyrimidine was involved in a bidentate hydrogen bond with the hinge directing the phenyl ring along the hinge with vectors out toward solvent (Figure 2). In

this binding mode, it was postulated that the methyl groups could make hydrophobic contacts with the Met129 gatekeeper, with the carbonyl oxygen lone pair recruiting the conserved catalytic lysine and/or aspartate. Based on this assumption, there were four main areas for substitution that were considered. Most of the examples presented below will focus on regions 1 and 4, while details around regions 2 and 3 will be discussed in the following paper.

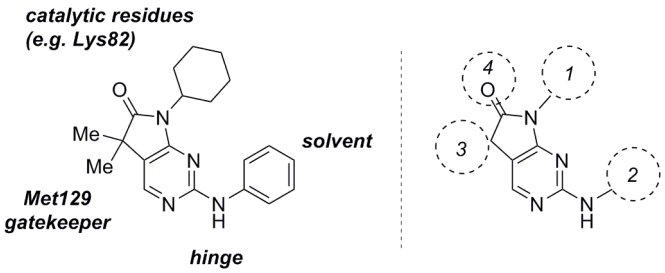

Figure 2. Vectors for further elaboration of **1**.

Initial structural changes to the lead were consistent with the original docking studies. For instance, substitution within or about the Ar ring (region 2) was rather permissive of polar functionality, (Table 1, piperidine **14** or 3-pyridyl **15**), which would be expected with a solvent-facing region. In general, substitution off of this aromatic ring delivered more potent analogs, albeit with no improvements in LE. However, more importantly this functional group tolerance allowed for fine tuning of physical properties, which will be discussed in more detail in the following communication. Similarly, changes to the lactam (region 4) completely eroded MARK activity, such as with the inverted isoindolinone **11** and the des-carbonyl pyrrolopyrimidine **13**, supporting the hypothesis that the lactam carbonyl was involved in H-bonding interactions with the catalytic residues.

Compound	MARK3 IC_{50} (nM)	LE	MARK4 Cell IC_{50} (nM)
14 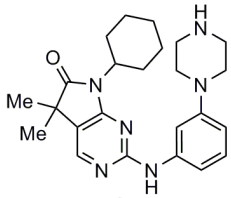	14	0.35	920
15 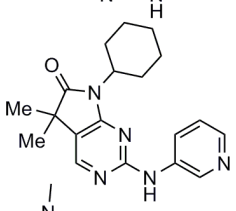	346	0.35	5,990
11 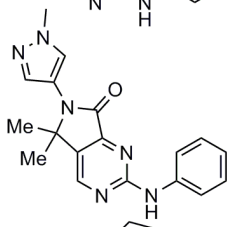	>30,000	NA	>10,000
13 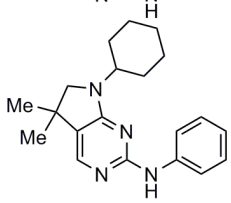	>30,000	NA	>10,000
16 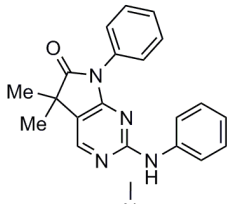	2,800	0.30	>10,000
17 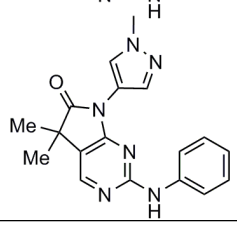	4,300	0.29	NA

Table 1: Initial SAR About the Pyrrolpyrimidone Core

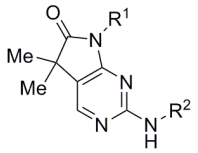

Compound	R^1	R^2	MARK3 IC_{50} (nM)	LE	MARK4 Cell IC_{50} (nM)
18			12,770	0.35	>10,000
19		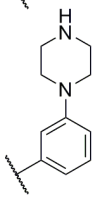	850	0.32	NA
20			3,000	0.36	NA
21			627	0.38	NA
22			226	0.36	NA
23	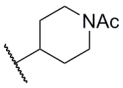		1,302	0.29	NA
24			117	0.41	5,910
25			738	0.36	>10,000
26	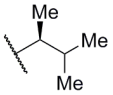		80	0.40	2,750
27	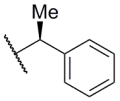		37	0.38	3,760
28	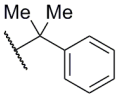		1,644	0.28	>10,000
29			2,564	0.36	>10,000
30	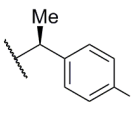	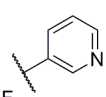	62	0.35	>10,000

Table 2: Deconstruction of the Cyclohexyl Group

In contrast, initial attempts to implement rational design in region 1 via modeling were less productive. For example, transformation of the cyclohexyl to the unsaturated phenyl analog **16** or the pyrazole **17** were predicted to be well tolerated, but resulted in >9x loss in potency vs. the cyclohexyl reference compound (Table 1). As a result, much of the early SAR in this region proceeded in a more empirical fashion. In fact, the initial SAR indicated the core of the initial hit seemed to represent an optimized minimal core (e.g. gem-dimethyl, carbonyl of the lactam, N-Aryl along hinge). However, it still remained to be determined how best to optimize the cyclohexyl fragment. In order to understand this more completely, it was decided to remove this piece entirely and evolve the lead back out into this space. To this end, removing the cyclohexyl piece completely, as with **18**, had a detrimental effect on the absolute potency, but the core still retained most of the binding efficiency (Table 2). Subsequent step-wise growth of the carbon chain, from the *N*-Me **19** (compare to **14**), to the ethyl and isopropyl analogs **20** and **21** respectively, hinted that it was possible to achieve a level of binding efficiency comparable to or better than the cyclohexyl starting point. One direction pursued was to install small, symmetrical ring systems, such as the cyclopentyl analog **22**. While this was generally tolerated, there were no obvious SAR breakthroughs with the initial analogs. For instance, attempts to incorporate heteroatoms into these ring systems, exemplified by the *N*-acyl piperidine **23** were accompanied with large drop-offs in potencies.

While the initial cyclic analog approach was not fruitful, extending out into the space with acyclic analogs proved to be more promising. Simply going from the isopryopyl analog **21** to the sec-butyl analog **24** resulted in a modest, but noticeable, increase in both potency and binding efficiency. Even more intriguing was the influence of stereochemistry at the alpha carbon, as the sec-butyl *R* isomer **25** was about 6 fold less potent. This preference for the *S* isomer in the acyclic analogs was shown to be rather general (>50x for some analogs, data not shown). As such, maintaining the alpha-methyl gearing element and continuing to grow off of the other position, such as with the *N*-3-methylbutan-2-yl **26** or the alpha-methyl-benzyl **27** resulted in a trend toward increased MARK potency with minimal sacrifices in binding efficiency. Attempts to explore the alpha position a little further, such as with the gem-dimethyl analog **28** or with the difluoromethyl **29** indicated that there was little room for further elaboration in this region. Docking studies on these compounds suggested that the alpha methyl group should be in close proximity to the glycine rich loop with minimal tolerance for substitution. In general, while slow progress was being made using this empirical SAR method, many of the more interesting leads suffered from poor cell activity (Table 1 & 2, MARK4 cell IC_{50}) and insufficient off-target kinase selectivity (data not shown), limiting their usefulness as tool compounds.

About this time, crystal structures of select compounds bound to the MARK2 enzyme became available. One example was the fluorobenzyl **30** (Figure 3), which confirmed many aspects of the proposed binding mode. As suspected, the aminopyridine was making contacts with the hinge regions and the pyridine ring was projecting out toward solvent. The gem-dimethyl groups were located near the Met129 gatekeeper residue and the carbonyl of the lactam ring was within H-bonding distance of the catalytic Lys82. While the fluorobenzyl group occupied the ribose region as expected, there were no obvious interactions present to explain much of the SAR in that region (*vide supra*). In particular, the importance of stereochemistry of the alpha methyl group was confounding, as the binding pocket appeared to be capable of accommodating both enantiomers.

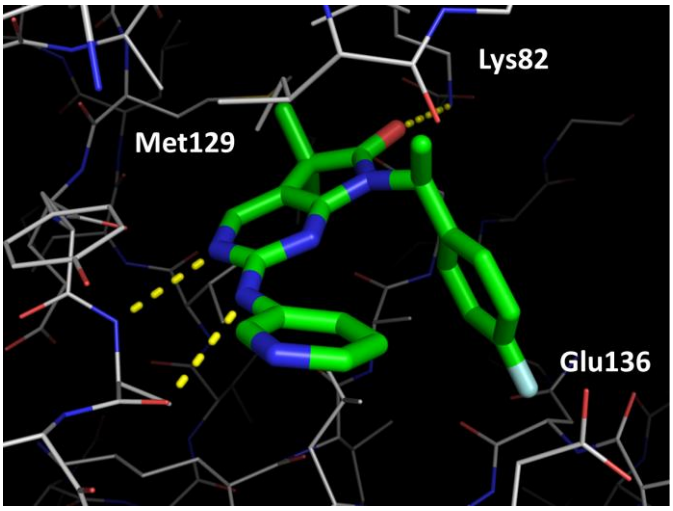

Figure 3. X-Ray structure of Compound **30** bound to MARK2. (PDB code: 5KZ7)

The structure of **30** did suggest two potential strategies to further increase the potency of these compounds. In the first case, the tolerance of certain cyclic analogs (e.g. **1** and **22**), and the crystal structure of **30** suggested that cyclization into a bicyclic structure (Figure 4) might lock the ligand in the bioactive conformation. A second approach was based on the proximity of the 3-position of the benzyl ring to Glu136 at the lip of the ATP binding pocket. It was possible that additional binding affinity could be gained by the proper placement of an acidic polar functionality at this position, as well as provide an additional handle for further modification of physical properties.

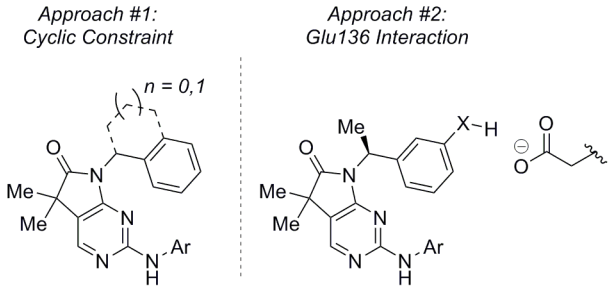

Figure 4: Target Strategy Based of the Structure of Compound **30**

In practice, both of these strategies proved to be effective. As can be seen in Table 3, cyclization (Approach #1) to the 5-membered indane **31** was well tolerated.(21) In order to explore approach #2, the meta phenol **32** was prepared, resulting in modest gains in MARK3 potency. However, a more substantial gain was observed when both approaches were combined into a single molecule, such as with the hydroxyindane **33**. A subsequent crystal structure of **33** bound to MARK2 (Figure 5) confirmed that the aromatic ring was placed in a similar orientation as observed in **31** and that the phenol was making additional interactions with Glu136. Subsequent modifications to probe this Glu136 interaction demonstrated that in many ways, the phenol was an optimized interaction, exemplified by a few select analogs included in Table 3. For instance adjusting the pKa with the aniline **34** resulted in ~10x drop-off in intrinsic potency. Similar modifications, such as with the sulfonamide **35** highlight the sensitivity at this region to combinations of pKa and the degree of the substitution. While these gains in potency/efficiency were exciting, it was equally satisfying to see that they were displaying reasonable levels of MARK cell activity.

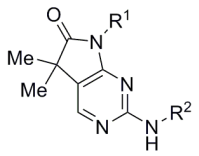

Compound	R^1	R^2	MARK3 IC_{50} (nM)	LBE	MARK4 Cell IC_{50} (nM)
31	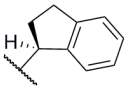		27	0.37	520
32	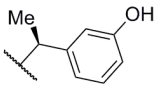		10	0.38	270
33	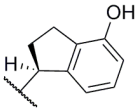		1.2	0.42	21
34	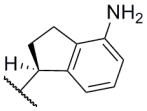		10	0.38	450
35	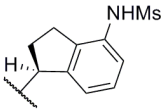		19	0.32	180

Table 3: Optimization From the Crystal Structure of **30**

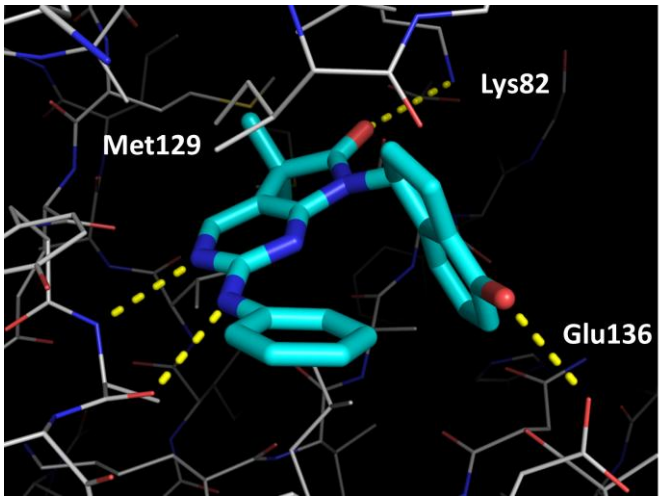

Figure 5. X-Ray structure of Compound **33** bound to MARK2. (PDB code: 5KZ8)

Compounds such as **33** proved to be useful tools to test the *in vitro* effects of selective MARK inhibitors. As detailed in Figure 6, **33** is one of the more potent and efficient MARK inhibitors profiled from this structural class, with excellent cell activity. In addition, optimization of key contacts from the crystal structures translated into selectivity across a subset of the kinome. While not exquisitely selective, only 5 kinases out of a panel of 10 kinases had activity <100 fold.(22) However, the pharmacokinetics of **33** are very poor, with high turnover in *in vitro* systems translating into high clearances and short half lives *in vivo*. In general, this was representative of this class of compounds, which hindered their subsequent development as *in*

vivo tool compounds for the program. The efforts to overcome this issue are described in the following communication.

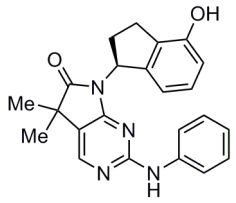

Compound **33**
MW = 386
LogD = 2.92
LE = 0.42
RLM $t_{1/2}$ = 9 min
HLM $t_{1/2}$ = 10 min

MARK3 IC_{50} = 1.2 nM
MARK4 Cell IC_{50} = 21 nM

5/100 kinases <100x (invitrogen):
NUAK1 = 5 nM
FLT3 = 8 nM
CSFR1 = 12 nM
KIT = 76 nM
AMPK = 98 nM

Rat PK:
Cl_p = 341 mL/min/kg
V_D = 16.2 L/kg
$t_{1/2}$ = 0.8 h

Dog PK:
Cl_p = 68 mL/min/kg
V_D = 4 L/kg
$t_{1/2}$ = 0.8 h

Figure 6. Properties of Compound **33**

In summary, we have described the development of an uHTS lead into a potent and selective MARK inhibitor. This was accomplished through a combination of targeted SAR based on initial binding hypotheses, and further refined by the use of insights gleaned from select X-ray structures. This ultimately allowed for the identification of suitable *in vitro* tool compounds such as **33**. However, the development of *in vivo* tools compounds was hindered by a complex series of PK issues that are described in the following manuscript.

Acknowledgements

We would like to thank Vincent Chevalier for his work on the IBX cyclization chemistry during a Co-Op Internship from Northeastern.

References and Notes

1. Querfurth, H. W.; LaFerla, F. M. *N. Engl. J. Med.* **2010**, *362*, 329. DOI: 10.1056/NEJMra0909142
2. Citron, M. *Nat. Rev. Drug Discov.* **2010**, *9*, 387. DOI:10.1038/nrd2896
3. Lee, V. M.-Y.; Brunden, K. R.; Hutton, M.; Trojanowski, J. Q. *Cold Spring Harb. Perspect. Med.* **2011**, 1. DOI: 10.1101/cshperspect.a006437
4. Martin, L.; Latypova, X.; Wilson, C. M.; Magnaudeix, A.; Perrin, M.-L.; Yardin, C.; Terro, F. *Ageing Res. Rev.* **2013**, *12*, 289. DOI:10.1016/j.arr.2012.06.003
5. Timm, T.; Marx, A.; Panneerselvam, S.; Mandelkow, E.; Mandelkow, E.-M. *BMC Neurosci.* **2008**, *9(Suppl 2)*, S9. DOI: 10.1186/1471-2202-9-S2-S9
6. Nishimura, I.; Yang, Y.; Lu, B. *Cell* **2004**, *116*, 671. DOI: 10.1016/S0092-8674(04)00170-9.
7. Wager, T.T.; Hou, X.; Verhoest P.R.; Villalobo, A. *ACS Chem. Neurosci.* **2010**;*1*:435. DOI: 10.1021/cn100008c
8. cLogD and PSA were calculated using ACD Labs. LE was calculated as LE = -[RT*ln(pIC_{50})] / N_{heavy}.
9. P-gp substrate susceptibility was assessed by measuring the BA:AB ratio in LLC-PK1 cells expressing complementary DNA (cDNA) encoding human MDR1 P-gp or rat Mdr1a P-gp.
10. The MARK3 activity was assessed in an HTRF-based assay utilizing full-lenth human MARK3 and an biotin labeled peptide substrate.
11. The MARK4 cell assay was conducted in HEK 293T cells stably transfected with human MARK4 and Tau protein. Quantitative change of phosphorylated tau protein at Ser 262 was measured using Perkin Elmer's technology AlphaLisa.
12. Note that for the purposes of this publication, we will make no distinction between any of the MARK isoforms. At the time, it was not anticipated that meaningful differences in isoforms could be achieved. Instead, efforts were focused on delivering a compound with sufficient protein kinase selectivity as a tool compound.
13. Yoshida, H.; Goedert M. J. *Neurochemistry* **2012**, *120*, 165. DOI: 10.1111/j.1471-4159.2011.07523.x
14. Haidle, A.; Stanton, M.; Altman, M.; Konrad, K.; Zabierek, A.; Katz, J.; Jewell, J. WO 20090152027 A1
15. Nicolaou, K.C.; Baran, P.S.; Zhong, Y.-L.; Sugita, K. *J. Am. Chem. Soc.* **2002**, *124*, 2212. DOI: 10.1021/ja012124x
16. Nicolaou, K.C.; Sugita, K.; Baran, P.S.; Zhong, Y.-L. *J. Am. Chem. Soc.* **2002**, *124*, 2221. DOI: 10.1021/ja012125p
17. Nicolaou, K.C.; Baran, P.S.; Zhong, Y.-L.; Barluenga, S.; Hunt, K.W.; Kranich, R.; Vega, J.A. *J. Am. Chem. Soc.* **2002**, *124*, 2233. DOI: 10.1021/ja012126h
18. Nicolaou, K.C.; Montagnon, T.; Baran, P.S.; Zhong, Y.-L. *J. Am. Chem. Soc.* **2002**, *124*, 2245. DOI: 10.1021/ja012127+
19. Nicolaou, K.C.; Baran, P.S.; Kranich, R.; Zhong, Y.-L.; Sugita, K.; Zou, N. *Angew. Chem. Int. Ed.* **2001**, *40*, 202. DOI: 10.1002/1521-3773(20010105)40:1<202::AID-ANIE202>3.0.CO;2-3
20. We briefly explored the generality of this transformation beyond the scope described in ref 11 to prepare highly substituted isoindolinones (V. Chevalier). Although the yield and scope were proven to be somewhat limited, this protocol could be used to access otherwise inaccessible functionality. Given the proposed mechanism, it was not surprising that a range of aromatic groups were tolerated about a simplified core, with yields ranging between 25-43%. Similarly, as described by Baran, electron rich aromatics capable of stabilizing the radical intermediate were required, but highlights that additional groups could be considered for this transformation.

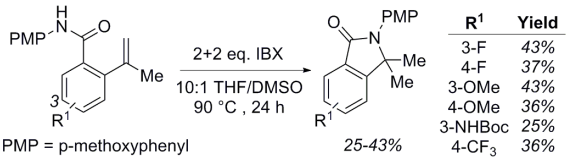

R^1	Yield
3-F	43%
4-F	37%
3-OMe	43%
4-OMe	36%
3-NHBoc	25%
4-CF_3	36%

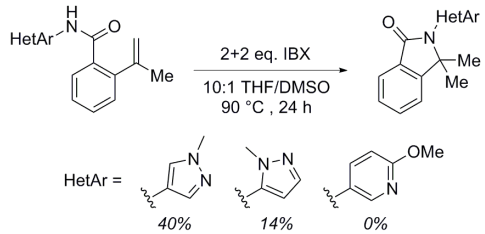

21. The stereochemistry was also important in the cyclic analogs (e.g. enantiomer of **32** IC_{50} = 1.8 μM). Other ring systems were also tolerated (e.g. racemic tetrahydronapthalene IC_{50} = 73 nM.
22. The full list is included as Supplemental Data. Off-target kinase values are estimated IC_{50} data from percent inhibition at three concentrations (0.1, 1, and 10 μM).